NASA/TM-2004-213264

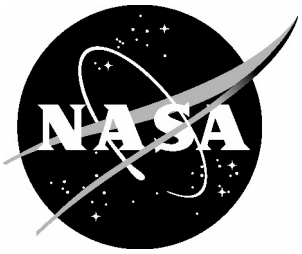

Determination of Extrapolation Distance With Measured Pressure Signatures From Two Low-Boom Models

Robert J. Mack and Neil Kuhn
Langley Research Center, Hampton, Virginia

November 2004

The NASA STI Program Office . . . in Profile

Since its founding, NASA has been dedicated to the advancement of aeronautics and space science. The NASA Scientific and Technical Information (STI) Program Office plays a key part in helping NASA maintain this important role.

The NASA STI Program Office is operated by Langley Research Center, the lead center for NASA's scientific and technical information. The NASA STI Program Office provides access to the NASA STI Database, the largest collection of aeronautical and space science STI in the world. The Program Office is also NASA's institutional mechanism for disseminating the results of its research and development activities. These results are published by NASA in the NASA STI Report Series, which includes the following report types:

- TECHNICAL PUBLICATION. Reports of completed research or a major significant phase of research that present the results of NASA programs and include extensive data or theoretical analysis. Includes compilations of significant scientific and technical data and information deemed to be of continuing reference value. NASA counterpart of peer-reviewed formal professional papers, but having less stringent limitations on manuscript length and extent of graphic presentations.

- TECHNICAL MEMORANDUM. Scientific and technical findings that are preliminary or of specialized interest, e.g., quick release reports, working papers, and bibliographies that contain minimal annotation. Does not contain extensive analysis.

- CONTRACTOR REPORT. Scientific and technical findings by NASA-sponsored contractors and grantees.

- CONFERENCE PUBLICATION. Collected papers from scientific and technical conferences, symposia, seminars, or other meetings sponsored or co-sponsored by NASA.

- SPECIAL PUBLICATION. Scientific, technical, or historical information from NASA programs, projects, and missions, often concerned with subjects having substantial public interest.

- TECHNICAL TRANSLATION. English-language translations of foreign scientific and technical material pertinent to NASA's mission.

Specialized services that complement the STI Program Office's diverse offerings include creating custom thesauri, building customized databases, organizing and publishing research results ... even providing videos.

For more information about the NASA STI Program Office, see the following:

- Access the NASA STI Program Home Page at ***http://www.sti.nasa.gov***

- E-mail your question via the Internet to help@sti.nasa.gov

- Fax your question to the NASA STI Help Desk at (301) 621-0134

- Phone the NASA STI Help Desk at (301) 621-0390

- Write to:

NASA STI Help Desk
NASA Center for AeroSpace Information
7121 Standard Drive
Hanover, MD 21076-1320

NASA/TM-2004-213264

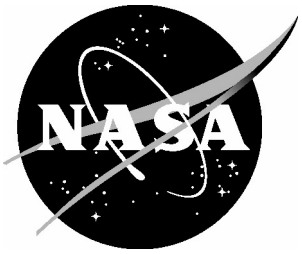

Determination of Extrapolation Distance With Measured Pressure Signatures From Two Low-Boom Models

Robert J. Mack and Neil Kuhn
Langley Research Center, Hampton, Virginia

National Aeronautics and
Space Administration

Langley Research Center
Hampton, Virginia 23681-2199

November 2004

Available from:

NASA Center for AeroSpace Information (CASI)
7121 Standard Drive
Hanover, MD 21076-1320
(301) 621-0390

National Technical Information Service (NTIS)
5285 Port Royal Road
Springfield, VA 22161-2171
(703) 605-6000

Summary

A study to determine a limiting distance-to-span ratio for the extrapolation of near-field pressure signatures is described and discussed. This study was to be performed in two wind-tunnel facilities with two wind-tunnel models. At this time, only the first half of the study has been completed, so the scope of this report is limited to the design of the models, and to an analysis of the first set of measured pressure signatures. The results from this analysis showed that pressure signatures with the desired "flat-top" low-boom shapes were not likely to be seen at separation distances less than 5 span lengths. While there were some indications that the pressure signature shapes were becoming more "flat-topped", this was not seen to be a strong trend at the distance- to-span ratios employed in this first series of wind-tunnel tests.

Introduction

There are currently two methods for extrapolating a near-field-measured or -predicted pressure signature to obtain a predicted ground overpressure. One is the Thomas Code, reference 1, and the other is the Ames Code, reference 2. If the pressure signature was generated by a slender body of revolution at zero lift and measured at a suitable separation distance, the Thomas Code or the Ames Code could be used with confidence to predict the ground overpressure from the original signature, separation distance, and the Mach number. That same ground overpressure could also be predicted by the Aeronautical Research Associates of Princeton (ARAP) Code, reference 3, from the body geometry, the cruise altitude, and the Mach number.

However, the situation is very different when the near-field pressure signature is generated by a lifting wing-body model in a wind tunnel or is predicted by a Computational Fluid Dynamics (CFD) code. In this situation, neither the Thomas Code nor the Ames Code can be appropriately applied. They are both based on a cylindrical acoustic propagation model; the first code was developed by Charles Thomas, and the second code was based on theories developed by G. B. Whitham and F. Walkden, references 4 and 5. The extrapolated ground overpressure signatures are usually very different in shape and character from ground overpressure signatures predicted with the ARAP code from concept or model volume and lift equivalent area descriptions.

There is another mathematical extrapolation technique called the Method of Multipoles, reference 6. With this method, an "extracted far-field" pressure signature is derived from overpressures calculated around a cylinder at one or more body lengths from the body or aircraft. Then, this "derived far-field" pressure signature is extrapolated to the ground with the Thomas Code to obtain a ground-level overpressure prediction.

Some of these near-field extrapolation methods are based on questionable assumptions. Whether the single near-field pressure signature is measured in the wind tunnel or calculated with a CFD code, it is a part of a fully three-dimensional flow field generated by a three-dimensional lifting model. Extrapolating this near-field pressure signature with a cylindrical, two-dimensional propagation code violates the physics of the flow field generated by the model's volume and lift contributions. If the separation distance were large enough, this objection would vanish.

The far-field pressure signature, extracted by the Method of Multipoles from the calculated near-field disturbances on a cylindrical surface around the model, is based on model geometry and its disturbances in the flow field. It is assumed that the body's geometry has been completely and faithfully represented,

and that the disturbances in the flow field have been accurately calculated. A wide variety of theory-prediction-measurement comparisons (Method of Multipoles predictions compared with Whitham theory predictions and wind-tunnel measurements, for example) has yet to be presented, especially for low-boom shaped pressure signatures. Obviously, a method must be found that is mathematically practical, but does not violate the physics of the flow field generated by the concept or wind-tunnel model. As yet, this method may not have appeared, or if it has, it has not been satisfactorily validated.

However, a limiting distance for credible extrapolation could be determined by the measurement of a large number of pressure signatures from wind-tunnel models. It would be the separation distance where the flow-field features of the overpressure signatures measured directly under the flight path of the model, have developed quasi-two-dimensional characteristics. This limiting distance could be expressed as a function of the span of a wing-body model since the lift is developed across the span even though the effects of this lift is felt in the flow field within the forward Mach conoid. By low-boom tailoring the model's geometry, the quasi-two-dimensional features of the pressure signature would be reasonably easy to identify.

A study to determine such a limiting distance ratio - distance/span - is described and discussed in this report. This study was planned to be performed in two wind-tunnel facilities, the Langley Research Center Unitary Plan Wind Tunnel Facility, and the John Glenn Research Center 10 Foot x 10 Foot Wind Tunnel Facility. At this time, only the first half has been completed, so the scope of this report is limited to the design of the models, and to an analysis of the pressure signatures measured under the flight path in the Langley Research Center Unitary Plan Wind Tunnel Facility. The totality of the wind-tunnel-measured pressure signature data is to be published in a separate report. When the second part of the study is completed, another report with all wind-tunnel-measured pressure signature data will be published. This follow-on report will have an analysis of the second data set, as well as the conclusions reached from a complete analysis of all the wind-tunnel-measured data.

Nomenclature

b	wing span, of models, 4.5 in
C_L	lift coefficient
$C_{L,CRUISE}$	lift coefficient at cruise
$F(y)$	value of Whitham F-function at effective distance y, $ft^{1/2}$
h	cruise altitude, ft
I	non dimensional pressure signature impulse, $I = \int_0^{\tau_o} \frac{\Delta p}{p} d\tau$
l	overall length of models, 9.0 in
l_e	effective length of the models at $C_{L,CRUISE}$, 9.0 in
M	Mach number
p	ambient pressure, psf
Δp	overpressure in the aircraft's flow field, psf
S	wing projected area, in^2
x	distance in the longitudinal direction, in
x_0	distance in the longitudinal direction where the impulse has a maximum value, in
y	distance in the spanwise direction normal to x, in, or effective distance, ft
τ	dimensionless dummy variable, x/l_e, in the equation of the impulse
τ_o	dimensionless ratio, x_o/l_e, along the pressure signature where the impulse has a maximum value

Concept and Model Design

Conceptual Vehicle

Two simplified concepts were designed for this study. The concepts had the same wing area, span, lifting length, and thickness-to-chord ratio. A horizontal tail and engine nacelles, canards, or fin(s) were not added to the configuration so that basic wing-fuselage volume and wing lift effects could be studied. These simplified configurations were low-boom tailored to produce a ground overpressure of 0.5 psf, the same ground overpressure that a recently-designed Supersonic Business Jet (SBJ) vehicle, reference 7, produced while cruising at a Mach number of 2.0, a beginning-cruise weight of 88,000 lb, and a beginning-cruise altitude of 53,000 feet.

The two concepts were different in that one concept had a wing with a smooth and continuous curved leading edge, the Curved Leading Edge (CLE) model, while the other concept had a wing with a straight-line segmented leading edge, the Straight-Line Segmented Leading Edge (SLSLE) model. These two wings, at full size, are shown for comparison in figure 1.

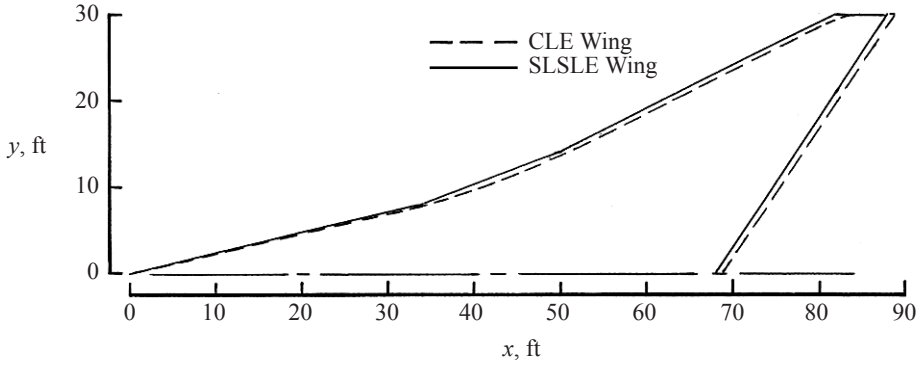

Figure 1. Full-scale wing planforms used for two wind-tunnel models.

Like the full-scale concepts, the wind-tunnel models had simplified wing and fuselage configurations. Sting area was added to the full-scale vehicles' lift equivalent area because it would be needed in the design of the wind-tunnel models. Using the code described in reference 8 that was developed from references 9 and 10, low-boom fuselages were contoured so the equivalent areas from the volumes of the wing, fuselage, and forward sting, along with the equivalent area due to wing lift, closely matched the equivalent area profile required for desired low-boom performance. A comparison of ideal and designed equivalent areas, F-functions, and ground pressure signatures for both concepts are presented in figures 2 to 4.

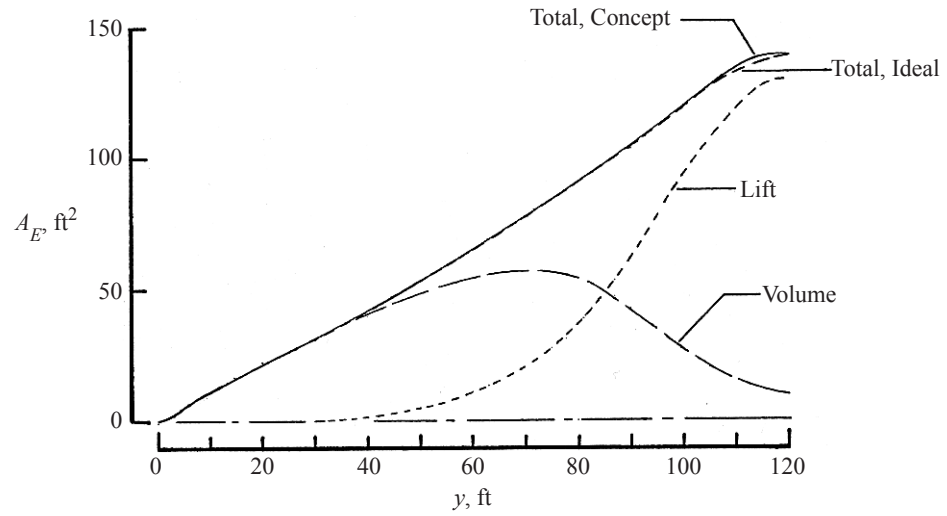

(a) Curved leading edge (CLE) concept.

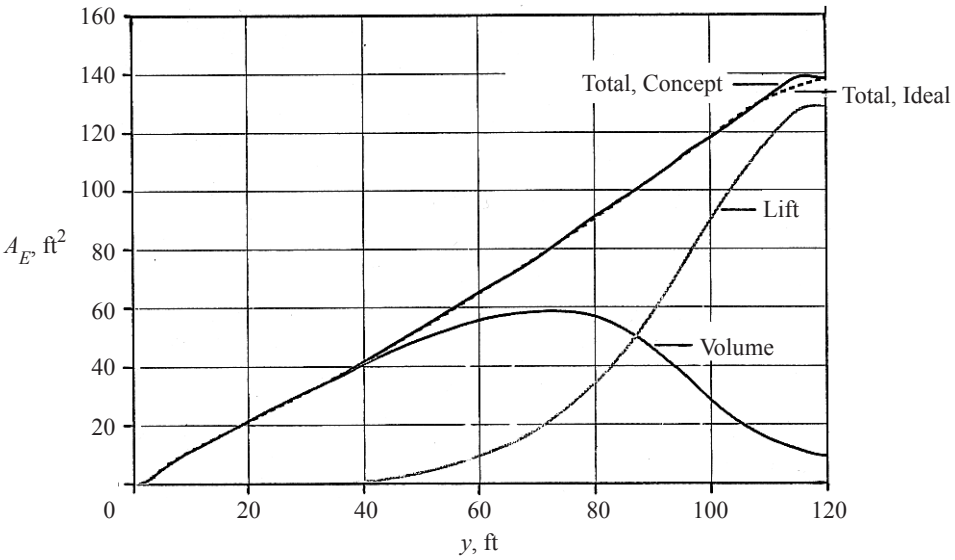

(b) Straight-line segmented leading edge (SLSLE) concept.

Figure 2. Comparison of ideal and designed equivalent areas.

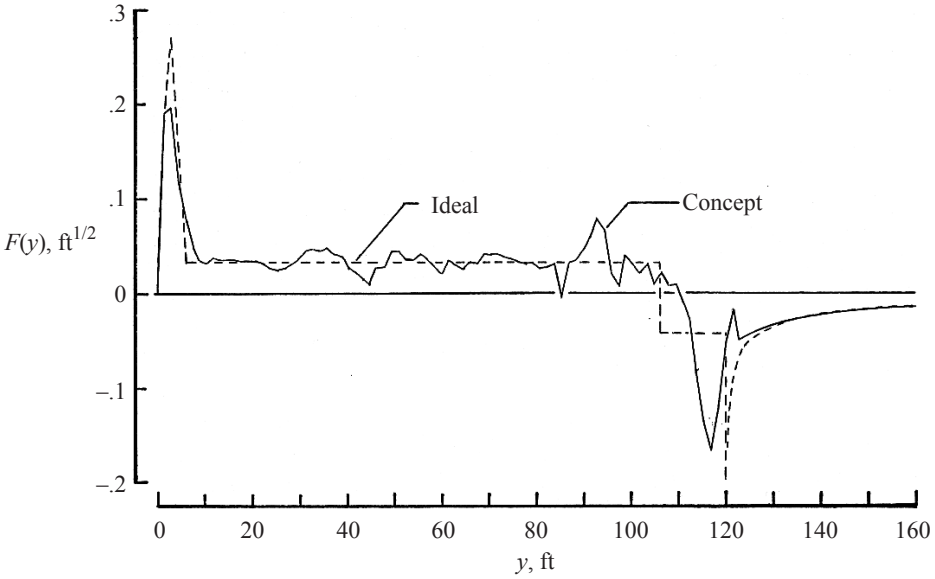

(a) Curved leading edge (CLE) concept.

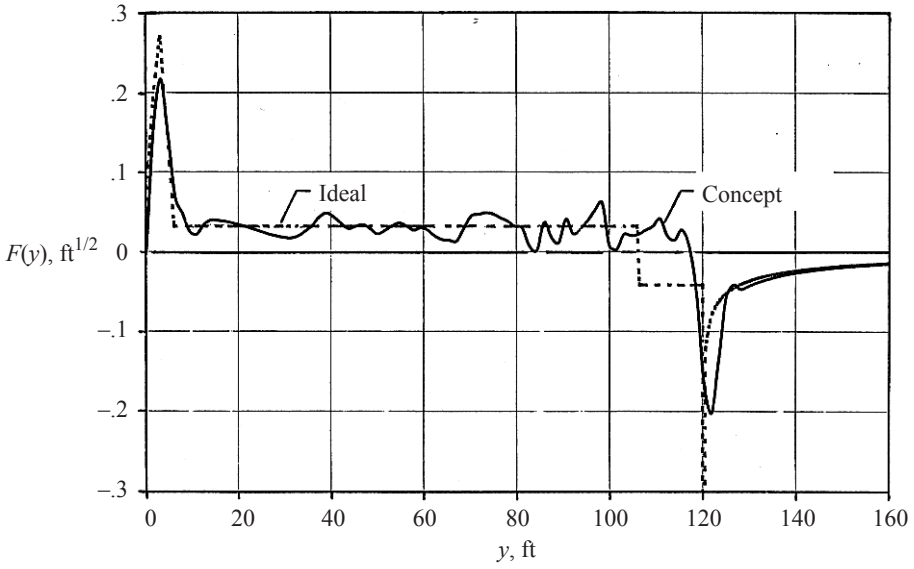

(b) Straight-line segmented leading edge (SLSLE) concept.

Figure 3. Comparison of ideal and designed F-functions.

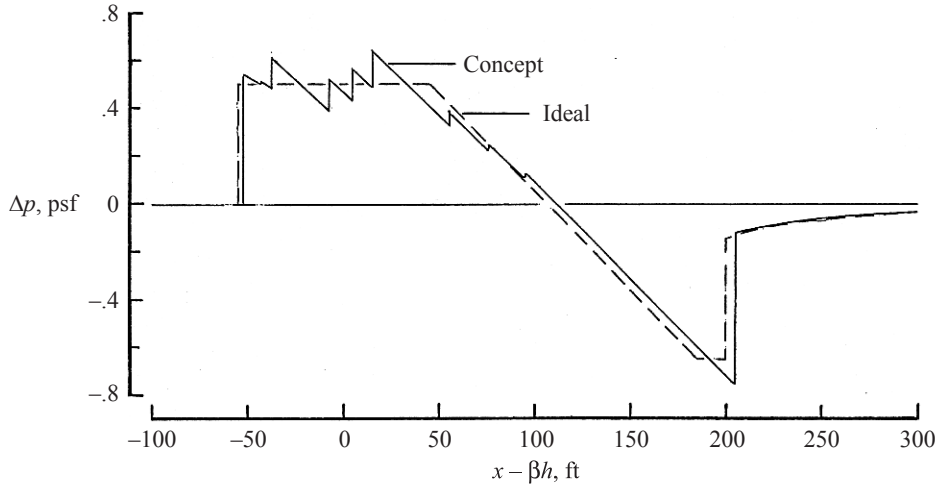

(a) Curved leading edge (CLE) concept.

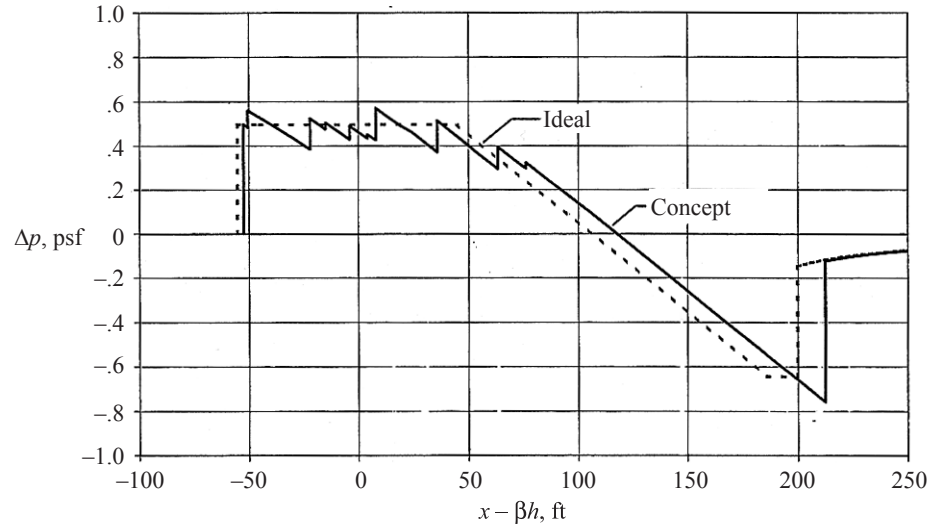

(b) Straight-line segmented leading edge (SLSLE) concept.

Figure 4. Comparison of ideal and designed ground overpressure signatures.

Wing dihedral, shown to be useful for achieving low-boom constraints in reference 11, was added to put the wing tip trailing edge and the model nose in a plane that was parallel with the direction of the free-stream velocity vector. This design feature made the overall length and the effective length of each model coincident at $C_{L,CRUISE}$.

Wind-Tunnel Model Design

After the research wing-fuselage concepts had been designed, they were rescaled by a factor of 1:160 so that practical wind-tunnel models could be built. These models were supported by a sting/balance whose cylindrical and tapered-cylinder contours merged with those on the models' aft fuselages. Each model and sting/balance was 32 inches in length with a 4-inch long, 0.75-inch diameter mounting stub at the back of the sting/balance. The front section of the CLE model with an extended cylindrical section is shown in figure 5.

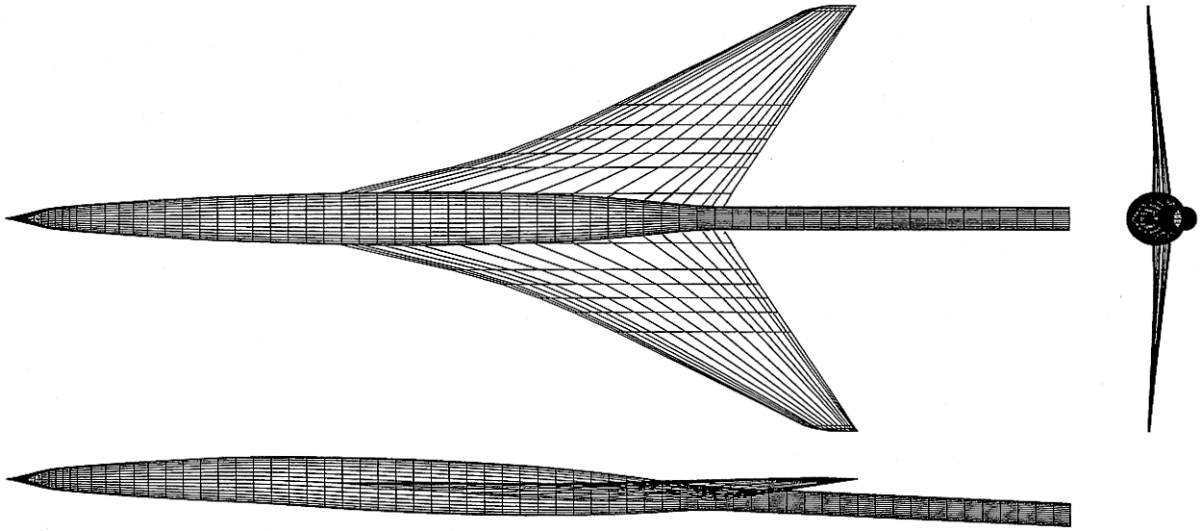

Figure 5. Three-view schematic of the CLE model.

The SLSLE model was similar to the CLE model in figure 5. This can be seen in the three-view schematic presented in figure 6.

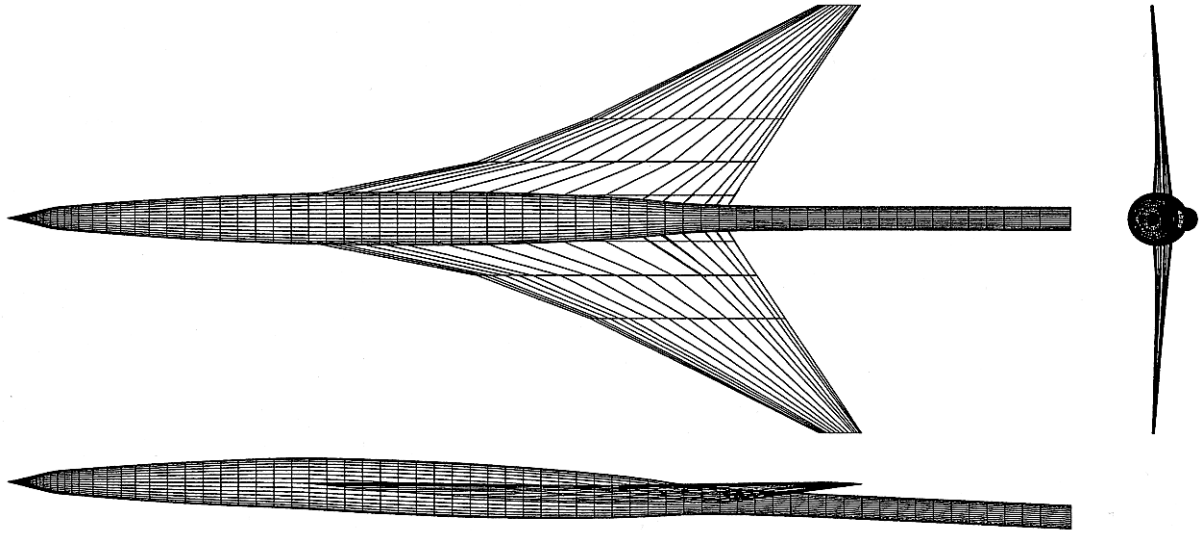

Figure 6. Three-view schematic of the SLSLE model.

Full-scale concept flight data and wind-tunnel model dimension and area data are listed in Appendix A. A numerical description in Harris Wave Drag code format, references 12 and 13, of each model is given in Appendix B and Appendix C.

Except for the leading edge shape, the two models were virtually identical. However, the leading edge shape was one of the questions addressed in this study. Seebass and George Minimization theory curves show a smooth and continuous growth of volume and lift equivalent areas for low-boom characteristics. Since the wing lift was such an important element in the total equivalent areas, it would be desirable for the lift development to have smooth and continuous gradients. This consideration strongly suggested that the wing be given a smoothly-curved, subsonic leading edge. However, it would be easier to mount leading edge flaps on a wing with a leading edge composed of straight-line segments than on a wing whose leading edge was curved from wing-fuselage junction to tip chord. If it could be demonstrated that a straight-line segmented wing leading edge, with small incremental changes in sweep, added few penalties to the low-boom ground overpressures, then the complexity of a curved leading edge wing for a prospective low-boom supersonic-cruise vehicle could be avoided.

Pressure Signature Measurements

Wind-Tunnel Test Section

Pressure signatures were measured with the models mounted on an angle-of-attack mechanism designed to control their lift by altering their angle of attack. This angle-of-attack mechanism was attached to the wind-tunnel strut mechanism which moved the model laterally to the desired separation distance, and then longitudinally, to permit measurement of the individual overpressures in the pressure signature. A schematic of this wind-tunnel test section arrangement of model and measurement apparatus is shown in figure 7.

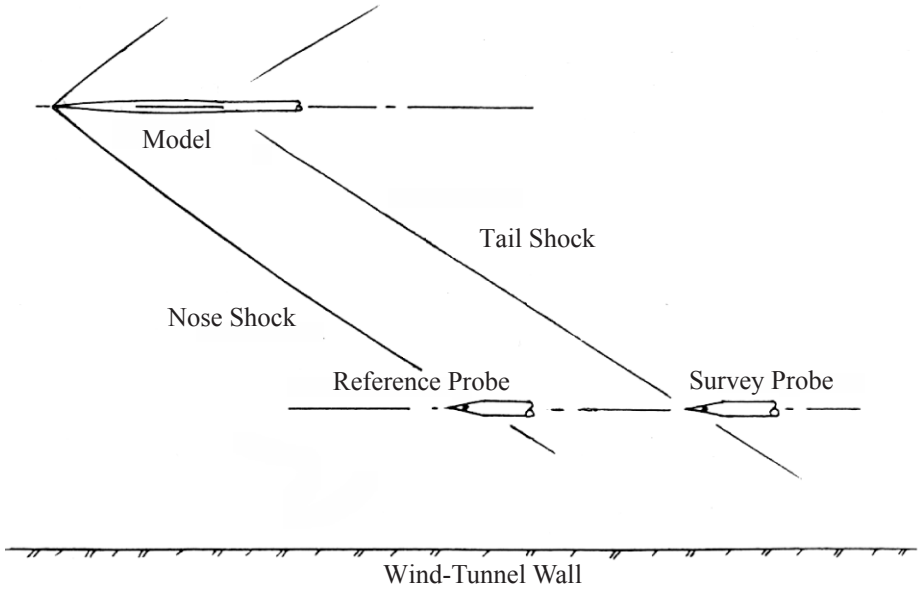

(a) Side view of model and probes.

Figure 7. Side view schematic of model and probes in the test section.

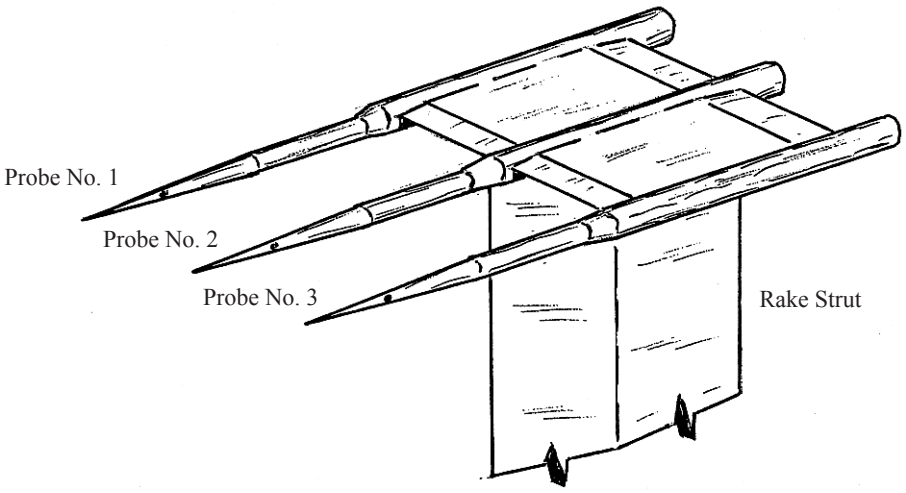

(b) Schematic of the survey probe rake and probes.

Figure 7. Concluded.

Three two-orifice conical probes were used to measure pressure signatures. They were side by side on a rake whose plane was normal to the model's vertical plane of symmetry. Probe No. 1 measured pressure signatures along a line 2.95 inches to the right of the model's flight path; Probe No. 2 measured signatures along a line directly under the model's flight path, and Probe No. 3 measured signatures along a line 6.35 inches to the left of the model's flight path. Probe No. 1 was located between Probe No. 2, and the static pressure reference probe. These "off-track" measured pressure signatures were data for present and future prediction code validation. In this report, only the under-the-flight track pressure signatures obtained with Probe No. 2 will be discussed and analyzed. The other data will be published in a separate data report.

Pressure Signature Measurement Matrix

Pressure signatures were measured at a Mach number of 2.0, and at number of separation distances to determine how, and at what rate, the pressure signature shapes changed. They were also measured at two values of $C_L/C_{L,CRUISE}$ to determine the influence and relative importance of lift on the shape of the pressure signature with increasing separation distance. A table of wind-tunnel model test data, presented in Appendix D, lists the separation distances in terms of span lengths, and the values of $C_L/C_{L,CRUISE}$ used to measure the pressure signatures generated by each of the models.

Pressure Signatures

A sample of the measured pressure signatures were analyzed, and their characteristics compared with theory. As was mentioned previously, only the pressure signatures measured under the model flight path, along with their significant analysis parameters, were presented and discussed in this report. The first comparison was between measured and predicted nose shock strengths. Second was a comparison between measured and predicted "impulse", i.e. the integral of overpressure ratio along the positive part of the pressure signature. The third comparison was between the measured signature shapes for both models at separation distance to span ratios, h/b , of 2.0 and 5.0, with $C_L/C_{L,CRUISE} = 1.0$.

Nose Shock Comparisons

Flow field shocks measured in the wind-tunnel test section were rounded instead of sharply abrupt. They were spread over a finite distance because of the finite-sized orifices in the conical probes, pressure disturbance propagation in the measurement probe's surface boundary layer, and model vibration due to wind-tunnel turbulence. A method for correcting these effects was presented and explained in reference 14. This pressure signature correction method is demonstrated in figure 8.

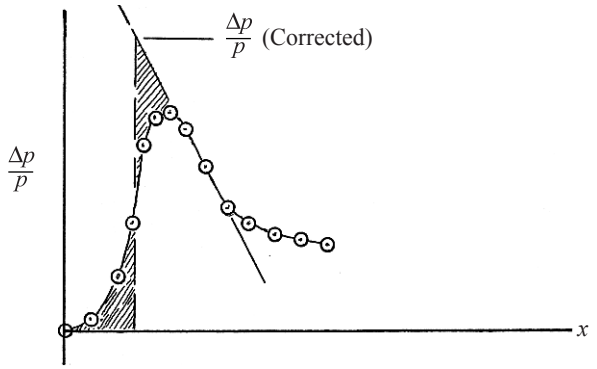

Figure 8. Typical wind-tunnel measured and corrected nose shock.

The corrected shock strength was obtained by preserving "impulse" (balancing the shaded areas) in the nose-shock region of the pressure signatures. Corrected nose shock parameters in far-field format, $(\Delta p/p)(h/l_e)^{3/4}$, were obtained for all the pressure signatures measured under the flight path at $C_L/C_{L,CRUISE} = 1.0$, and were compared with theory in figure 9.

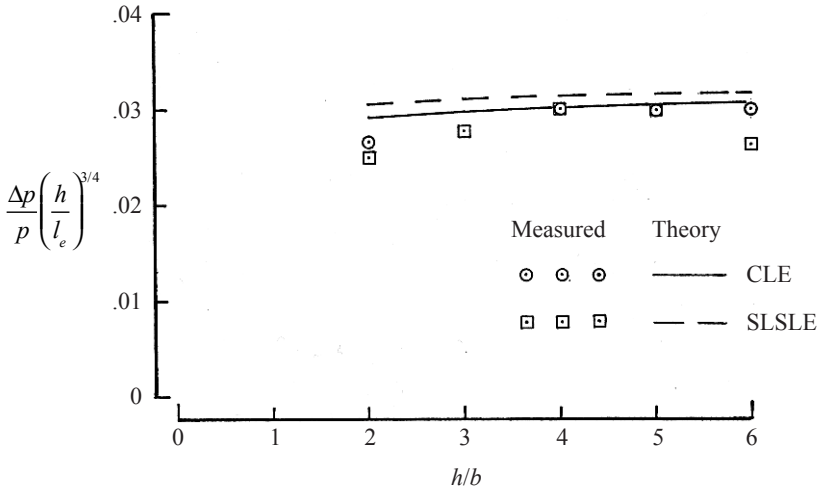

Figure 9. Comparison of corrected and theoretical nose shock parameters versus h/b for both wind-tunnel models. $CL/C_{L,CRUISE} = 1.0$, and M = 2.

This corrected nose shock overpressure parameter, plotted in figure 9, should asymptotically approach a far-field value as h/b is increased. At a minimum limiting distance, the pressure signature could be extrapolated with the Thomas code. (The estimation of this distance was the second purpose of this

study.) With the exception of the one SLSLE data point at $h/b = 6$, the measured and corrected nose shock overpressures were seen to be approaching, but had not reached, a far-field value within the Unitary Plan Wind Tunnel 4 ft by 4 ft test section.

Impulse Comparisons

The impulse of the pressure signature is the integral of the positive part of pressure signature. So, no corrections need be applied to rounded shocks if their strengths are relatively weak, i.e. $\Delta p/p < 0.05$, across the pressure rise. The impulse from the under-the-flight-path measured pressure signatures are compared with theory in figure 10.

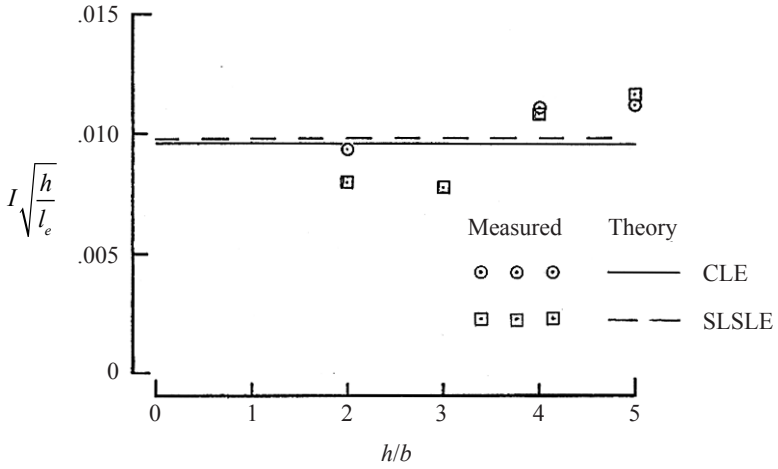

Figure 10. Comparison of theoretical and measured impulse versus h/b for both wind-tunnel models. $C_L/C_{L,CRUISE} = 1.0$, and M = 2.

Note that again, in figure 10, the impulse was expressed in far-field parameters, just as the over-pressure ratio was in figure 9. The abscissa has values that extend only as far as $h/b = 5$. With the probe in its most forward position, only the nose shock and first 3.0 to 4.0 inches of the pressure signature could be measured before the model's nose moved out of the test section into the aft section of the wind-tunnel nozzle where the flow was non-uniform.

Although the impulse data straddled the theory lines, the convergence trends in figure 10 were not as positive as those of the nose shock strengths in figure 9. This seemed to suggest that the limiting value of h/b for credible extrapolation would be considerably larger than 5 or 6.

Pressure Signature Shape

As was mentioned at the start of this report, this study was to determine where the pressure signature had become "sufficiently far-field" so that it could be extrapolated to the ground with the Standard Atmosphere Propagation version of the Thomas Code. The closest and the farthest near-field under-the-flight-path separation distances for obtaining complete signatures in the Unitary Plan Wind Tunnel were 9.0 inches and 22.5 inches respectively. Pressure signatures measured at these and the rest of the separation distances are presented in figures 11 to 17.

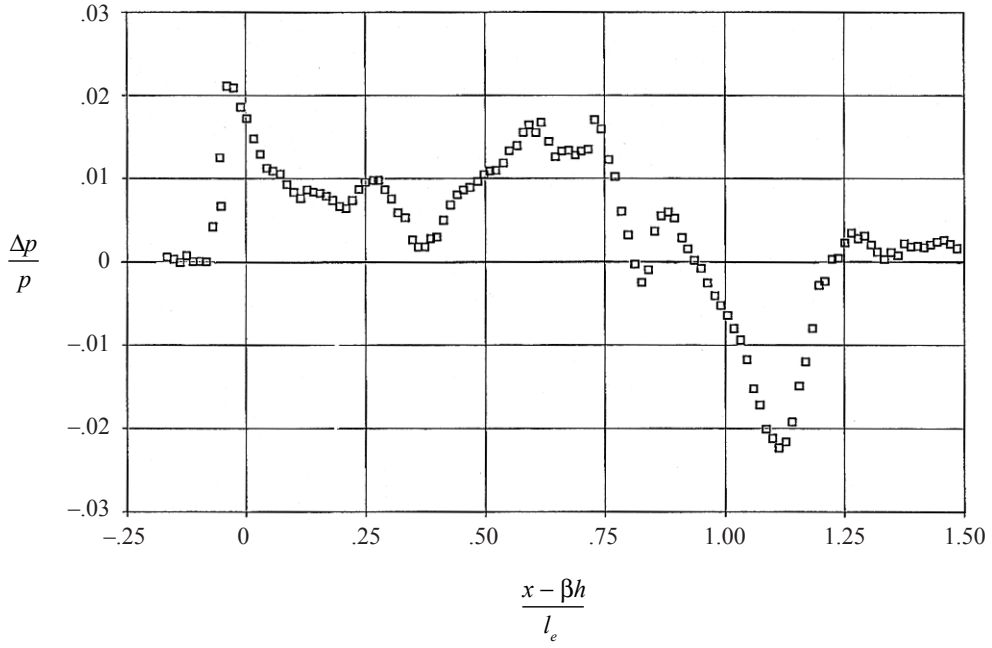

Figure 11. CLE model at M = 2, h = 9.0 inches, and $C_L/C_{L,CRUISE}$ = 1.0.

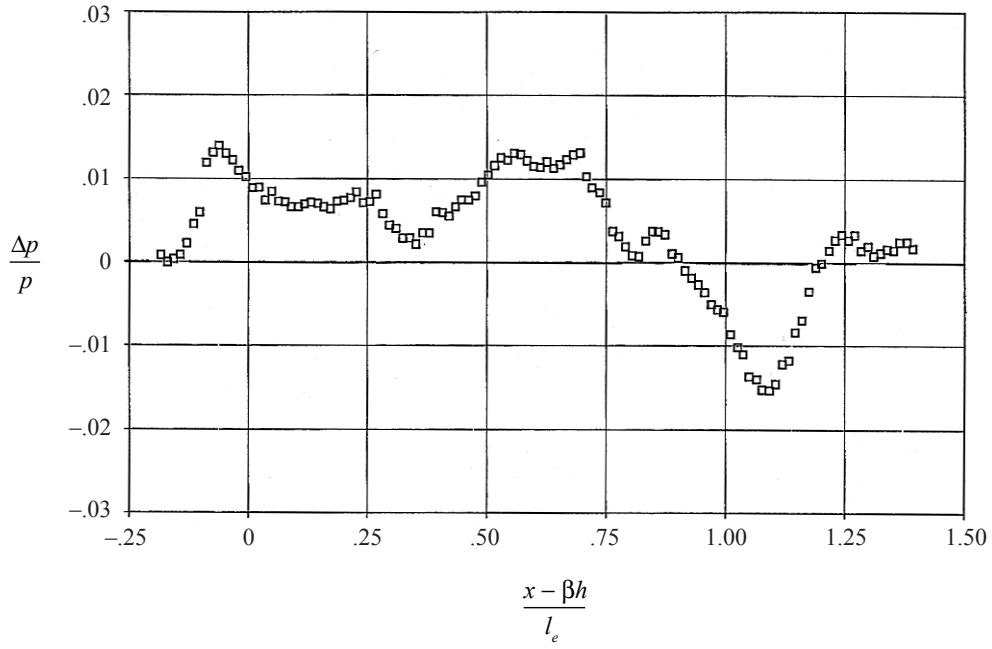

Figure 12. CLE model at M = 2, h = 18.0 inches, and $C_L/C_{L,CRUISE}$ = 1.0.

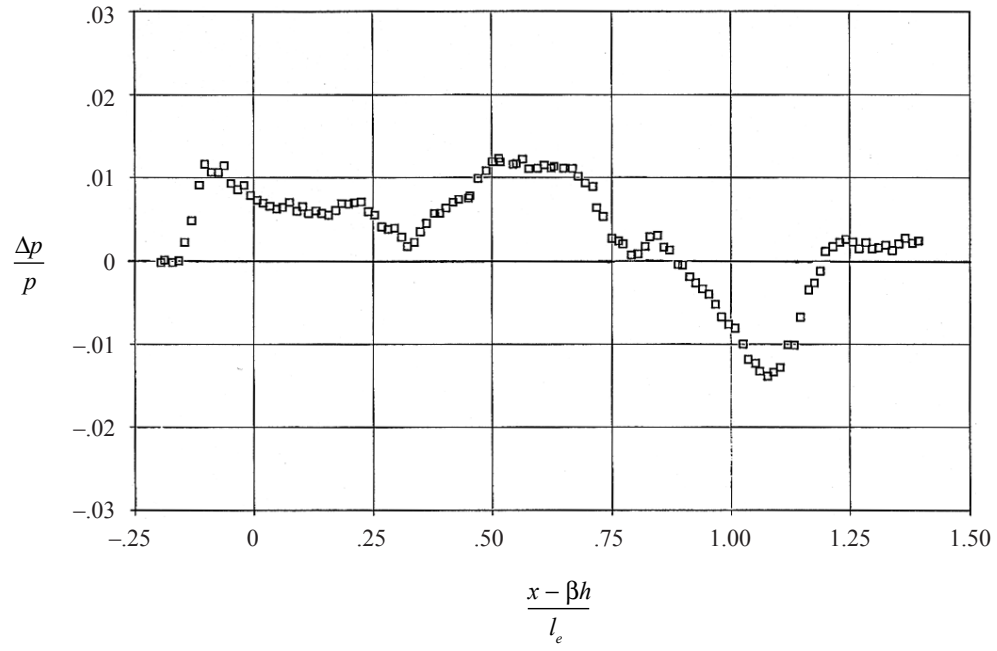

Figure 13. CLE model at M = 2, h = 22.5 inches, and $C_L/C_{L,CRUISE}$ = 1.0.

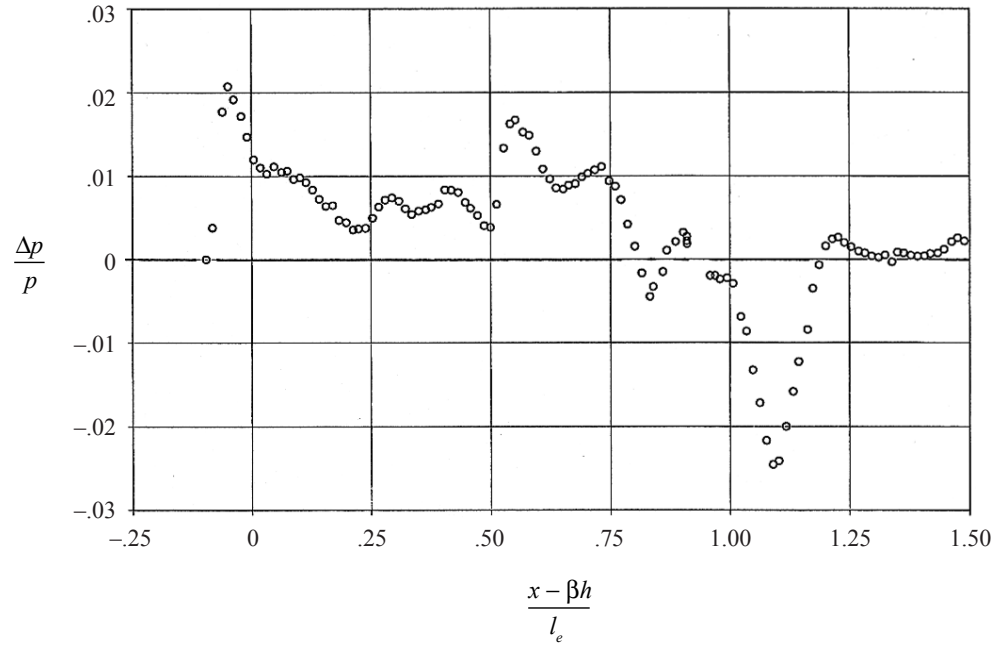

Figure 14. SLSLE model at M = 2, h = 9.0 inches, and $C_L/C_{L,CRUISE}$ = 1.0.

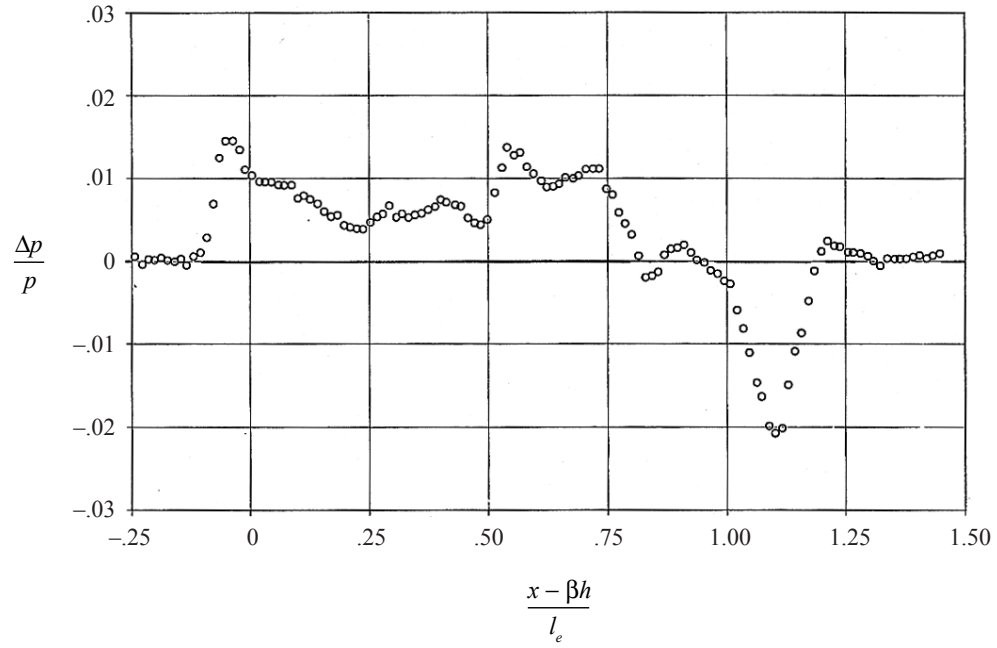

Figure 15. SLSLE model at M = 2, h = 13.5 inches, and $C_L/C_{L,CRUISE}$ = 1.0.

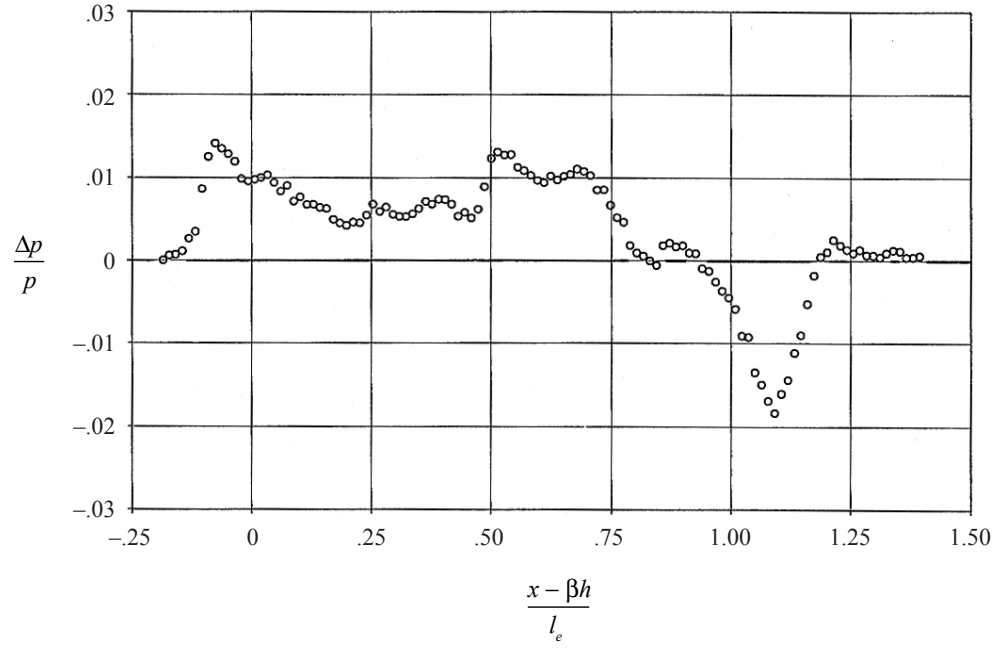

Figure 16. SLSLE model at M = 2, h = 18.0 inches, and $C_L/C_{L,CRUISE}$ = 1.0.

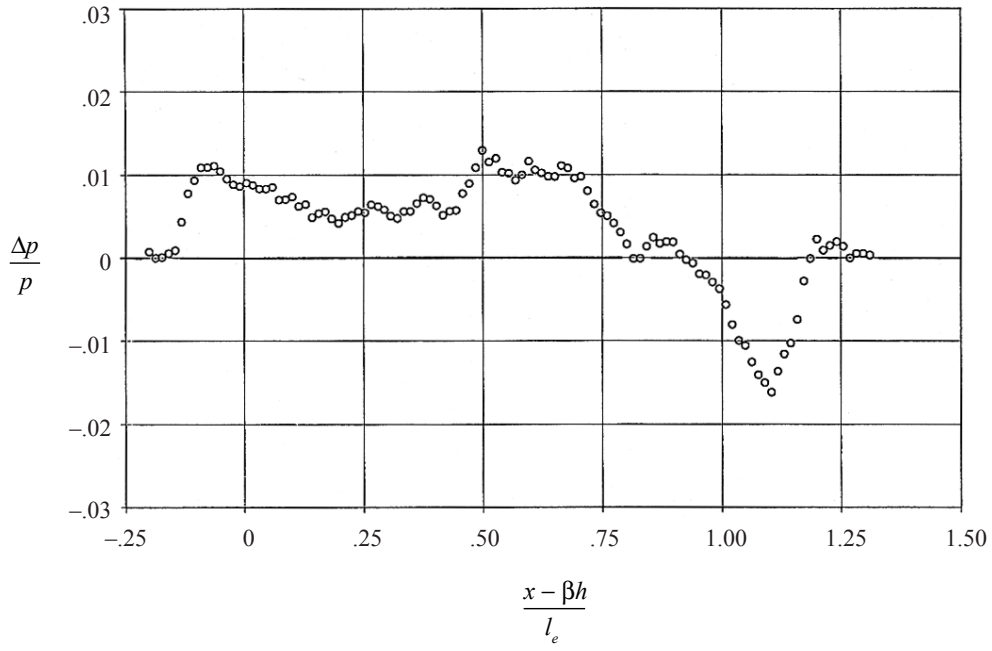

Figure 17. SLSLE model at M = 2, h = 22.5 inches, and $C_L/C_{L,CRUISE}$ = 1.0.

None of these pressure signatures has a "flat-top" shape, but the observed slow changes in shape are in that direction. Pressure signatures from both models at the closest and the farthest separation distances are shown superimposed in figures 18 and 19 for comparison purposes.

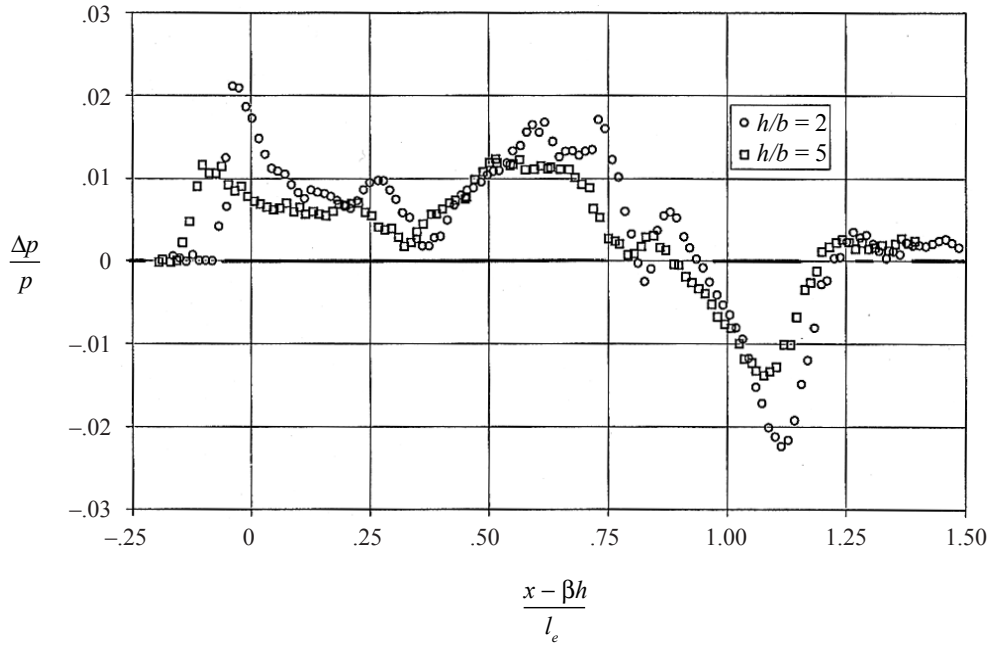

Figure 18. CLE model at M = 2, h = 9.0 and 22.5 inches, and $C_L/C_{L,CRUISE}$ = 1.0.

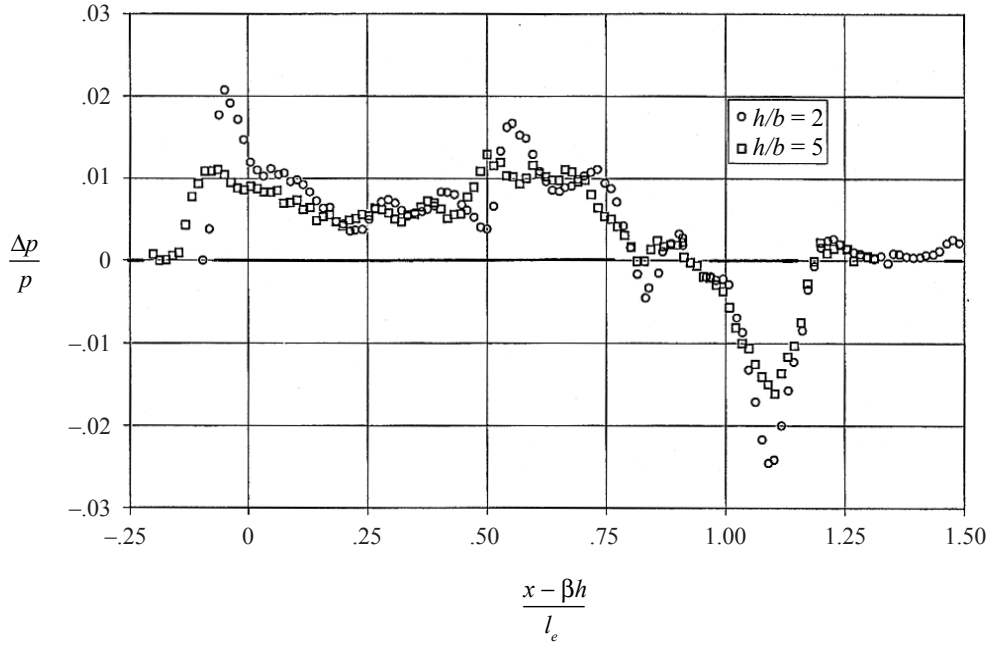

Figure 19. SLSLE model at M = 2, h = 9.0 and 22.5 inches, and $C_L/C_{L,CRUISE}$ = 1.0.

As would be expected, the pressure signatures at h = 22.5 inches are longer, due to attenuation, than those at h = 9.0 inches in both figures 18 and 19. The nose shock strengths on the pressure signatures in both figures also show an expected reduction due to attenuation. Also noticeable was the smoother and rounder maximum overpressure disturbances due to wing lift with the increased separation distance. Mini-shocks in the pressure signature measured at the closest separation distance have attenuated, but have not shown any tendencies to move forward with increasing distance toward coalescence with the nose shock.

The overpressures between the nose and the lift-induced shocks have changed little relative to the strengths of these two shocks. This trend would suggest that the pressure signatures would become smoother and more level as the separation distance increased. It is very likely that, on the ground, the pressure signature would probably have the design-goal shape with an almost-flat top along the positive-overpressure section.

Discussion

An inspection of the pressure signatures in figures 11 through 17 would suggest that the design goals shown in figures 4(a) and 4(b) had not been achieved. Not one of the pressure signatures generated by the two wind-tunnel models had the intended “flat-top” shape. However, both of the pressure signatures shown in figures 4(a) and 4(b) are far-field signatures. So, it is not too surprising that their shapes were not achieved at the near-field separation distances available in the Langley Unitary Plan Wind Tunnel Facility test section. It also indicates that the additional planned tests at larger separation distances in a larger wind-tunnel test section will need to be performed before definite conclusions can be made.

Comparisons of pressure signatures measured at 2 and 5 span lengths, figures 18 and 19, present a more optimistic picture. Especially since, in this first part of a two-part study, every one of these measured pressure signatures was a near-field pressure signature. In addition to indications from the pressure signatures shown in figures 11 through 17, the trends in nose-shock strength and impulse change

with increasing separation distance, seen in figures 9 and 10, shows that there is reason for the guarded optimism.

These results are in agreement with preliminary data presented in reference 15. That wind-tunnel data showed that a wind-tunnel model whose configuration was low-boom tailored might need separation distances of far more than 4 to 5 span lengths before the pressure signature began to show strong evidence of having a low-boom shape. However, that same report showed that a configuration with *approximate* low-boom tailoring would generate pressure signatures whose shape would show near-field features over very long distances. Both sets of data from those models put the results from these wind-tunnel measurements in a favorable light.

Concluding Remarks

None of the pressure signatures measured in this first half of a two-part study to determine a minimum distance for the extrapolation of pressure signatures to the ground had a distinctive "flat-top" shape. Thus, the results of the analysis of this first set of data indicated that pressure signatures with "flat-top" shapes were not seen in the ensemble of pressure signatures measured in the 2 to 5 span length near field region of the wind-tunnel test section. There were definite indications that the pressure signature shapes were becoming more "flat-topped" at the maximum separation distance of 5 span lengths. This trend toward the "flat-top" pressure signature was not seen to be strong, and was in accordance with results that have been seen before in previous wind-tunnel measurements of near-field pressure signatures from low-boom-tailored models. However, it is anticipated that in the second half of the study, the pressure signatures generated by the two models at considerably farther separation distances will show much more definite trends toward having far-field characteristics.

References

1. Thomas, Charles L.: *Extrapolation Of Sonic Boom Pressure Signatures By The Wave Form Parameter Method*. NASA TN D-6832, 1972.

2. Hicks, Raymond M.; and Mendoza, Joel P.: *Prediction Of Aircraft Sonic Boom Characteristics From Experimental Near Field Results*. NASA TM X-1477, September 1967.

3. Hayes, Wallace D.; Haefeli, Rudolph C.; and Kulsrud, H. E.: *Sonic Boom Propagation In A Stratified Atmosphere, With Computer Program*. NASA CR-1299, 1969.

4. Whitham, G. B.: *The Flow Pattern of a Supersonic Projectile*. Communications on Pure and Applied Mathematics vol. V, no. 3, August 1952, pp. 301-348.

5. Walkden, F.: *The Shock Pattern of a Wing-Body Combination, Far From the Flight Path*. Aeronautical Quarterly, vol. IX, pt. 2, May 1958, pp. 164-194.

6. Page, Juliet A.; and Plotkin, Kenneth J.: *An Efficient Method For Incorporating Computational Fluid Dynamics Into Sonic Boom Prediction*. AIAA 91-3275, AIAA 9th Applied Aerodynamics Conference, September 23-25, 1991.

7. Mack, Robert J.: *A Supersonic-Cruise Business Jet Concept Designed For Low Sonic Boom*. NASA/TM-2003-212435, October 2003

8. Mack, Robert J.; and Haglund, George T.: *A Practical Low-Boom Overpressure Signature Based On Minimum Sonic Boom Theory*. High-Speed Research: Sonic Boom, Volume II,NASA Conference Publication 3173, 1992.

9. Seebass, R.; and George, A. R.: *Sonic-Boom Minimization.* Journal of the Acoustical Society of America, vol. 51, no. 2, pt. 3, February 1972, pp. 686 - 694.

10. Darden, Christine M.: *Sonic Boom Minimization With Nose-Bluntness Relaxation.* NASA TP-1348, 1979.

11. Mack, Robert J.; and Darden, Christine M.: *Wind-Tunnel Investigation Of The Validity Of A Sonic-Boom-Minimization Concept*. NASA TP-1421, 1979.

12. Harris, Roy V., Jr.: *A Numerical Technique For Analysis Of Wave Drag At Lifting Conditions*. NASA TN D-3586, 1966.

13. Craidon, Charlotte B.: *Description Of A Digital Computer Program For Airplane Configuration Plots*. NASA TM X-2074, 1970.

14. Carlson, Harry W.: *Correlation Of Sonic-Boom Theory With Wind-Tunnel And Flight Measurements*. NASA TR R-213, December 1964.

15. Mack, Robert J.: *Persistence Characteristics of Wind-Tunnel Pressure Signatures From Two Similar Models*. NASA/TM-2004-212671. January 2004.

Appendix A

Description of the Two Wind-Tunnel Models

	SLSLE Model	CLE Model
Span, in	4.5	4.5
Effective length, in	9.0	9.0
Lift length, in	9.0	9.0
Wing area, in_2	10.08	10.0737
Mean aerodynamic chord, in	2.9615	2.9728
Aspect ratio, b^2/S	2.0	2.0

The following data pertains to the wings and the fuselages of full-scale vehicles. The wind-tunnel models used in the tests to measure pressure signatures were reduced-scale versions of these conceptual wing fuselages with the aft fuselage modified to blend into the sting.

	SLSLE Concept	CLE Concept
Cruise altitude, ft	53,000.0	53,000.0
Beginning cruise weight, lb	88,000.0	88,000.0
Beginning cruise wing loading, psf	49.386	49.386
Beginning cruise C_L	0.08309	0.08309
Cruise Mach number	2.0	2.0
Ground-level overpressure, psf	0.50	0.50
Ground-level reflection factor	1.90	1.90
Type of overpressure shape	“Flat-top”	“Flat-top”

Appendix B

Numerical Description of the Curved Leading-Edge Model (Lengths in ft, areas in ft^2)

```
Curved Leading Edge Wing Model, Flat Wing, Cambered Fuselage
  1  1 -1  0  0  0  0  9 17  3 19 30 19 30 19 10
1790.88                                                                                                  REF AREA
0.0    2.5    5.0    10.0   15.0   20.0   30.0   40.0   50.0   60.0                                      X AF 1
70.0   80.0   85.0   90.0   95.0   97.5   100.0                                                          X AF 2
46.561 3.50   -.4867 55.7722                                                                           WAFORG1
62.800 7.20   -.6226 42.0000                                                                           WAFORG2
70.000 9.20   -.6639 36.1333                                                                           WAFORG3
75.200 11.2   -.6171 32.2667                                                                           WAFORG4
80.000 13.2   -.5528 28.8000                                                                           WAFORG5
86.000 16.0   -.4311 24.6667                                                                           WAFORG6
112.40 29.2   0.2258 7.06667                                                                           WAFORG7
113.60 29.6   0.2281 6.13333                                                                           WAFORG8
116.00 30.0   0.1776 4.00000                                                                           WAFORG9
0.0    -.0619 -.1238 -.2476 -.3714 -.4953 -.7429 -.9905 -1.238 -1.486                                   ZORD1
-1.733 -1.981 -2.105 -2.229 -2.352 -2.414 -2.476                                                       ZORD1
0.0    -.0466 -.0932 -.1865 -.2797 -.3730 -.5594 -.7459 -.9324 -1.119                                   ZORD2
-1.305 -1.492 -1.585 -1.678 -1.772 -1.818 -1.865                                                       ZORD2
0.0    -.0401 -.0802 -.1604 -.2406 -.3209 -.4813 -.6417 -.8022 -.9626                                   ZORD3
-1.123 -1.283 -1.364 -1.444 -1.524 -1.564 -1.604                                                       ZORD3
0.0    -.0358 -.0716 -.1433 -.2149 -.2865 -.4298 -.5731 -.7163 -.8596                                   ZORD4
-1.003 -1.146 -1.218 -1.289 -1.361 -1.397 -1.433                                                       ZORD4
0.0    -.0320 -.0640 -.1278 -.1918 -.2557 -.3836 -.5115 -.6394 -.7672                                   ZORD5
-.8951 -1.023 -1.087 -1.151 -1.215 -1.247 -1.279                                                       ZORD5
0.0    -.0274 -.0548 -.1095 -.1643 -.2190 -.3286 -.4381 -.5476 -.6571                                   ZORD6
-.7666 -.8762 -.9309 -.9857 -1.040 -1.068 -1.095                                                       ZORD6
0.0    -.0078 -.0157 -.0314 -.0471 -.0628 -.0941 -.1255 -.1569 -.1883                                   ZORD7
-.2196 -.2510 -.2667 -.2823 -.2981 -.3059 -.3138                                                       ZORD7
0.0    -.0068 -.0136 -.0272 -.0408 -.0545 -.0817 -.1089 -.1362 -.1634                                   ZORD8
-.1906 -.2179 -.2315 -.2451 -.2587 -.2655 -.2723                                                       ZORD8
0.0    -.0044 -.0089 -.0178 -.0266 -.0355 -.0533 -.0710 -.0888 -.1066                                   ZORD9
-.1243 -.1421 -.1510 -.1598 -.1687 -.1732 -.1776                                                       ZORD9
0.0    .1560  .3040  .5760  .8160  1.024  1.344  1.536  1.600  1.536                                    WAF1
1.344  1.024  .8160  .5760  .3040  .1560  0.0                                                          WAF1
0.0    .1560  .3040  .5760  .8160  1.024  1.344  1.536  1.600  1.536                                    WAF2
1.344  1.024  .8160  .5760  .3040  .1560  0.0                                                          WAF2
0.0    .1560  .3040  .5760  .8160  1.024  1.344  1.536  1.600  1.536                                    WAF3
1.344  1.024  .8160  .5760  .3040  .1560  0.0                                                          WAF3
0.0    .1560  .3040  .5760  .8160  1.024  1.344  1.536  1.600  1.536                                    WAF4
1.344  1.024  .8160  .5760  .3040  .1560  0.0                                                          WAF4
0.0    .1560  .3040  .5760  .8160  1.024  1.344  1.536  1.600  1.536                                    WAF5
1.344  1.024  .8160  .5760  .3040  .1560  0.0                                                          WAF5
0.0    .1560  .3040  .5760  .8160  1.024  1.344  1.536  1.600  1.536                                    WAF6
1.344  1.024  .8160  .5760  .3040  .1560  0.0                                                          WAF6
0.0    .1560  .3040  .5760  .8160  1.024  1.344  1.536  1.600  1.536                                    WAF7
1.344  1.024  .8160  .5760  .3040  .1560  0.0                                                          WAF7
0.0    .1560  .3040  .5760  .8160  1.024  1.344  1.536  1.600  1.536                                    WAF8
1.344  1.024  .8160  .5760  .3040  .1560  0.0                                                          WAF8
0.0    .1560  .3040  .5760  .8160  1.024  1.344  1.536  1.600  1.536                                    WAF9
1.344  1.024  .8160  .5760  .3040  .1560  0.0                                                          WAF9
0.0    1.0    2.0    3.0    4.0    5.0    6.0    7.0    8.0    9.0                                      X FUSE1
10.0   12.0   14.0   16.0   18.0   20.0   22.5   25.0   27.5   30.0                                     X FUSE2
32.50  35.00  37.50  40.00  42.50  45.00  47.50  50.00  52.50  55.00                                    X FUSE3
0.0    0.0    0.0    0.0    0.0    0.0    0.0    0.0    0.0    0.0                                      Z FUS1
0.0    0.0    0.0    0.0    0.0    0.0    0.0    0.0    0.0    0.0                                      Z FUS2
-.0125 -.05   -.1125 -.2    -.308  -.418  -.528  -.638  -.748  -.858                                    Z FUS3
0.0    .18247 .72988 1.6490 2.9316 4.6568 6.3794 7.7191 8.8141 9.8145                                   FUS AREA1
10.869 12.819 14.780 16.763 18.781 20.718 23.157 25.518 28.086 30.339                                   FUS AREA2
32.271 34.108 35.891 37.719 39.258 40.942 42.545 43.826 44.651 45.365                                   FUS AREA3
55.00  57.50  60.00  62.50  65.00  67.50  70.00  72.50  75.00  77.50                                    X FUS4
80.00  82.50  85.00  87.50  90.00  92.50  95.00  97.50  100.0  102.5                                    X FUS5
105.0  107.5  110.0  112.5  115.0  117.5  120.0  122.5  125.0  127.5                                    X FUS6
-.858  -.968  -1.078 -1.188 -1.298 -1.408 -1.518 -1.628 -1.738 -1.848                                  Z FUS4
-1.958 -2.068 -2.178 -2.288 -2.398 -2.508 -2.618 -2.728 -2.838 -2.948                                  Z FUS5
-3.058 -3.168 -3.278 -3.388 -3.498 -3.608 -3.718 -3.828 -3.938 -4.048                                  Z FUS6
45.365 45.365 45.365 44.651 44.226 43.179 41.854 40.264 38.265 35.944                                   FUS AREA4
33.336 30.288 26.970 23.243 19.494 15.834 12.378 10.010 8.8141 8.5530                                   FUS AREA5
8.5530 8.5530 8.5530 8.5530 8.5530 8.5530 8.5530 8.5530 8.5530 8.5530                                   FUS AREA6
127.5  130.0  132.5  135.0  137.5  140.0  142.5  145.0  147.5  149.857                                  X FUS7
-4.048 -4.158 -4.268 -4.378 -4.488 -4.598 -4.708 -4.818 -4.928 -5.0317                                 Z FUS7
8.5530 8.5530 8.5530 8.5530 8.5530 8.5530 8.5530 8.5530 8.5530 8.5530                                   FUS AREA7
   12000  96  24   2                 000                                                               AOA
32.0   80.00                                                                                           XREST
```

Appendix C

Numerical Description of the Straight-Line-Segment Leading-Edge Model (Lengths in ft, areas in ft^2)

```
Straight Line Segmented Leading Edge Wing Model, Flat Wing, Cambered Fuselage
  1  1 -1  0  0  0  0  4 17  3 19 30 19 30 19  9
1792.00                                                                    REF AREA
0.0    2.5    5.0    10.0   15.0   20.0   30.0   40.0   50.0   60.0      X AF 1
70.0   80.0   85.0   90.0   95.0   97.5   100.0                           X AF 2
42.20  3.25   -.098  59.9666                                              WAFORG1
66.00  8.00   -.3888 39.3333                                              WAFORG2
82.00  14.0   -.3739 27.3333                                              WAFORG3
114.0  30.0   0.1073 6.00000                                              WAFORG4
0.0    -.065  -.130  -.259  -.389  -.519  -.778  -1.037 -1.297 -1.556    ZORD1
-1.815 -2.075 -2.204 -2.334 -2.464 -2.529 -2.5934                         ZORD1
0.0    -.0451 -.0902 -.1804 -.2706 -.3608 -.5412 -.7216 -.9020 -1.0834   ZORD2
-1.2627-1.4431-1.5333-1.6235-1.7137-1.7588-1.8039                         ZORD2
0.0    -.0313 -.0627 -.1254 -.1881 -.2507 -.3761 -.5015 -.6269 -.7522    ZORD3
-.8776 -1.003 -1.0656-1.1283-1.1910-1.2224-1.2537                         ZORD3
0.0    -.0069 -.0138 -.0275 -.0413 -.0550 -.0825 -.1100 -.1376 -.1651    ZORD4
-.1926 -.2201 -.2338 -.2476 -.2613 -.2682 -.2751                          ZORD4
0.0    .1560  .3040  .5760  .8160  1.024  1.344  1.536  1.600  1.536     WAF1
1.3440 1.024  .8160  .5760  .3040  .1560  0.0                             WAF1
0.0    .1560  .3040  .5760  .8160  1.024  1.344  1.536  1.600  1.536     WAF2
1.3440 1.024  .8160  .5760  .3040  .1560  0.0                             WAF2
0.0    .1560  .3040  .5760  .8160  1.024  1.344  1.536  1.600  1.536     WAF3
1.3440 1.024  .8160  .5760  .3040  .1560  0.0                             WAF3
0.0    .1560  .3040  .5760  .8160  1.024  1.344  1.536  1.600  1.536     WAF4
1.3440 1.024  .8160  .5760  .3040  .1560  0.0                             WAF4
0.0    1.0    2.00   3.00   4.00   5.00   6.00   7.00   8.00   9.00      X FUSE 1
10.0   12.0   14.0   16.0   18.0   20.0   22.5   25.0   27.5   30.0      X FUSE 2
32.50  35.00  37.50  40.00  42.50  45.00  47.50  50.00  52.50  55.00     X FUSE 3
0.0    0.0    0.0    0.0    0.0    0.0    0.0    0.0    0.0    0.0       ZFUS1
0.0    0.0    0.0    0.0    0.0    0.0    0.0    0.0    0.0    0.0       ZFUS2
0.0001 -.0030 -.0150 -.0480 -.1080 -.2152 -.3221 -.4296 -.5368 -.6440    ZFUS3
0.0000 0.1839 0.7355 1.6548 2.9419 4.5968 6.6194 8.1209 9.1201 9.9878    FUS AREA1
10.934 12.888 14.908 16.973 19.065 21.165 23.775 26.340 28.830 31.217    FUS AREA2
33.477 35.586 37.523 39.272 40.814 42.136 43.227 44.076 44.677 45.023    FUS AREA3
55.00  57.50  60.00  62.50  65.00  67.50  70.00  72.50  75.00  77.50      X FUS4
80.00  82.50  85.00  87.50  90.00  92.50  95.00  97.50  100.0  102.5      X FUS5
105.0  107.5  110.0  112.5  115.0  117.5  120.0  122.5  125.0  127.5      X FUS6
-.6440 -.7511 -.8583 -.9655 -1.0727-1.1799-1.2871-1.3943-1.5015-1.6087   Z FUS4
-1.7159-1.8231-1.9302-2.0374-2.1446-2.2518-2.3590-2.4662-2.5734-2.6806   Z FUS5
-2.7878-2.8950-3.0022-3.1094-3.2165-3.3237-3.4309-3.5382-3.6457-3.7525   Z FUS6
45.023 45.119 45.050 44.785 44.125 43.075 41.715 40.059 38.128 35.945    FUS AREA4
33.535 30.931 28.167 25.050 21.350 17.419 14.395 12.400 11.100 10.200    FUS AREA5
9.6000 9.2000 8.8570 8.6530 8.5530 8.5530 8.5530 8.5530 8.5530 8.5530    FUS AREA6
127.5  130.0  132.5  135.0  137.5  140.0  142.5  145.0  149.265           X FUS7
-3.7525-3.8597-3.9669-4.0741-4.1813-4.2885-4.3956-4.5028-4.6856           Z FUS7
8.5530 8.5530 8.5530 8.5530 8.5530 8.5530 8.5530 8.5530 8.5530           FUS AREA7
   12000  96   24   2                  000                                AOA
32.0   80.00                                                              XREST
```

Appendix D

Wind-Tunnel Pressure Signature Measurement *h*/*b* and $C_L/C_{L,CRUISE}$ Values Under-the-Track Data

h, inches	*h*/*b*	$C_L/C_{L,CRUISE}$	Model
9.00	2.00	0.5, 1.0	SLSLE, CLE
13.50	3.00	0.5, 1.0	SLSLE, **
18.00	4.00	0.5, 1.0	SLSLE, CLE
22.50	5.00	0.5, 1.0	SLSLE, CLE
27.00	6.00	0.5, 1.0	SLSLE, CLE***

The Span, b, of both models was 4.5 inches

The initials SLSLE represent the model with a straight-line segmented leading edge.

The initials CLE represent the model with a curved leading edge that was smoothly continuous.

** Pressure signatures generated by the CLE model at a model-No. 2 probe separation distance of 13.5 inches (*h/b* = 3.0) were part of the schedule. However, the track mechanism that moved the three-probe measurement rake became inoperative before CLE model pressure signature measurements at *h/b* = 3.0 could be performed.

***Only forward section of the pressure signature measured. At this point in the signature measurement, the model noses were already slightly forward of the test section and into the aft section of the wind-tunnel nozzle where non-uniform Mach number gradients and flow angularities exist.

REPORT DOCUMENTATION PAGE

Form Approved
OMB No. 0704-0188

1. REPORT DATE *(DD-MM-YYYY)*	2. REPORT TYPE	3. DATES COVERED *(From - To)*
01- 11 - 2004	Technical Memorandum	

4. TITLE AND SUBTITLE

Determination of Extrapolation Distance With Measured Pressure Signatures From Two Low-Boom Models

5a. CONTRACT NUMBER

5b. GRANT NUMBER

5c. PROGRAM ELEMENT NUMBER

6. AUTHOR(S)

Mack, Robert J.; and Kuhn, Neil

5d. PROJECT NUMBER

5e. TASK NUMBER

5f. WORK UNIT NUMBER

23-065-10-91

7. PERFORMING ORGANIZATION NAME(S) AND ADDRESS(ES)

NASA Langley Research Center
Hampton, VA 23681-2199

8. PERFORMING ORGANIZATION REPORT NUMBER

L-19040

9. SPONSORING/MONITORING AGENCY NAME(S) AND ADDRESS(ES)

National Aeronautics and Space Administration
Washington, DC 20546-0001

10. SPONSOR/MONITOR'S ACRONYM(S)

NASA

11. SPONSOR/MONITOR'S REPORT NUMBER(S)

NASA/TM-2004-213264

12. DISTRIBUTION/AVAILABILITY STATEMENT

Unclassified - Unlimited
Subject Category 05
Availability: NASA CASI (301) 621-0390

13. SUPPLEMENTARY NOTES

An electronic version can be found at http://techreports.larc.nasa.gov/ltrs/ or http://ntrs.nasa.gov

14. ABSTRACT

A study to determine a limiting distance to span ratio for the extrapolation of near-field pressure signatures is described and discussed. This study was to be done in two wind-tunnel facilities with two wind-tunnel models. At this time, only the first half had been completed, so the scope of this report is limited to the design of the models, and to an analysis of the first set of measured pressure signatures. The results from this analysis showed that the pressure signatures measured at separation distances of 2 to 5 span lengths did not show the desired low-boom shapes. However, there were indications that the pressure signature shapes were becoming “flat-topped”. This trend toward a “flat-top” pressure signatures shape was seen to be a gradual one at the distance ratios employed in this first series of wind-tunnel tests.

15. SUBJECT TERMS

Sonic boom; Whitham theory, Signature extrapolation; Wind-tunnel models

16. SECURITY CLASSIFICATION OF:			17. LIMITATION OF ABSTRACT	18. NUMBER OF PAGES	19a. NAME OF RESPONSIBLE PERSON
a. REPORT	b. ABSTRACT	c. THIS PAGE			STI Help Desk (email: help@sti.nasa.gov)
					19b. TELEPHONE NUMBER *(Include area code)*
U	U	U	UU	28	(301) 621-0390